SYSTEM IDENTIFICATION AND ROBUST CONTROL FOR THE LNLS UVX FAST ORBIT FEEDBACK

D. O. Tavares#, LNLS, Campinas, Brazil
D. R. Grossi, São Paulo University, São Carlos, Brazil

Abstract

This paper describes the optimization work carried out to improve the performance of the LNLS UVX storage ring fast orbit feedback system. Black-box system identification techniques were applied to model the dynamic behavior of BPM electronics, orbit correctors, communication networks and vacuum chamber eddy currents. Robust control techniques were employed to analyze and optimize closed-loop performance and robustness.

INTRODUCTION

The LNLS storage ring FOFB system has been operating for users since March 2013. RMS stability integrated from 1 Hz to 500 Hz is 1% beam size in the horizontal plane and 6% for vertical in worst case (1% coupling is assumed). Disturbances originating on floor vibrations account for less than 0.2% RMS in horizontal plane and 2.5% RMS in vertical plane. The dominant disturbance source to be attenuated by the FOFB system is Elliptically Polarizing Undulator (EPU) gap/phase variations, while orbit disturbances caused by power supply ripple (up to 5% beam size, in vertical plane) should not be significantly amplified. The following sections describe the approach adopted to optimize the system performance and robustness.

HARDWARE DESCRIPTION

The LNLS FOFB system is a multiple-input multiple-output feedback control system comprising 48 sensors (24 beam position readings per transverse plane) and 42 actuators (18 horizontal orbit correctors + 24 vertical orbit correctors) running at 3.125 kHz update rate.

The data acquisition and control system hardware is composed of one central real-time controller (PXI-8108) and 12 data acquisition nodes (CompactRIO-9144 EtherCAT chassis) with analog and digital interface modules. Each acquisition/actuation node has an FPGA available for digital filtering, currently used for decimation (from 100 kS/s oversampling to 3.125 kS/s) and dynamic response compensation for each BPM reading and orbit correct current setpoint. Two daisy chain EtherCAT networks are used as deterministic network for sensor and actuator data distribution to/from the controller and provides synchronization between all nodes below 1 µs. Bergoz MX-BPM electronics are used for RF signals processing and delivers analog signals proportional to the beam position. In-house developed power supplies with analog interface and analog current regulator (Proportional-Integral type) are used to drive the orbit corrector magnets [1].

#daniel.tavares@lnls.br

SYSTEM IDENTIFICATION

Figure 1 depicts the general structure adopted for modeling the LNLS FOFB system using Laplace and Z transforms.

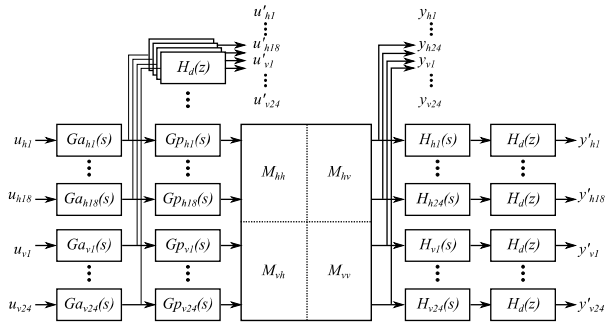

Figure 1: LNLS FOFB model structure.

The description of transfer functions and signals are given below:

- $Ga_{pj}(s)$: power supply + magnet impedance response of the j-th corrector of the p transverse plane (h = horizontal, v = vertical).
- $Gp_{pj}(s)$: magnet core + vacuum chamber magnetic field response (eddy currents) to coil current variations on the j-th corrector of the p plane.
- $H_{pi}(s)$: BPM electronics response of the i-th BPM of the p plane.
- $H_d(z)$: decimation filter response (discrete-time) at lower data rate (FOFB update rate) + communication network delay. Identical response for both BPM position reading and orbit corrector current reading.
- M_{p1p2}: static orbit response matrices ($p1$ plane BPMs and $p2$ plane orbit correctors). Horizontal and vertical plane matrices are represented by M_{hh} and M_{vv}, respectively. Crosstalk matrices (off-diagonal) are represented by M_{hv} and M_{vh}.
- u_{pj}: orbit corrector current setpoint (j-th corrector, p plane).
- u'_{pj}: orbit corrector current reading (j-th corrector, p plane).
- y_{pi}: actual beam position (i-th BPM, p plane).
- y'_{pi}: measured beam position (i-th BPM, p plane).

For black-box system identification the available ports for experiments comprise the discrete-time input signals u_{pj} and output signals u'_{pj} and y'_{pi}, with 320 µs sampling period. $H_d(z)$ transfer function is accurately known *a priori*, since it is fully determined by CIC decimation filters (factor 32 decimation rate, 2 sections and 1 differential delay) implemented in the nodes' FPGAs and one-cycle time delay due to the EtherCAT network data distribution.

ISBN 978-3-95450-148-9

Static orbit response matrices are readily obtained through the traditional method of small amplitude (tens of μrad) bipolar steps on each orbit corrector. For all purposes of this paper, M_{plp2} will be assumed to be known, including their variations due to known optics changes: ±2% tune shifts and extreme values of insertion device gap and phase configurations during normal operation.

Experiments

After experimenting with different types of excitation signals (white noise, sum of sinusoids, PRBS), a choice has been made for the pseudo-random binary signal (PRBS) due to its appropriate spectral content, easiness of use and periodicity enabling time-domain average of the experimental data. Special care has been taken to choose the sequence length in such a way that no major spectral line of the beam position readings and orbit corrector current readings (mainly due to magnets power supply ripple) aligned with some of the excitation harmonics. Figure 2 shows the chosen excitation pattern (62 points sequence, 750 Hz bandwidth, 9.2 μrad peak-to-peak excitation) in time-domain and frequency domain. For illustration, the beam position spectrum of a particular BPM is plotted in background.

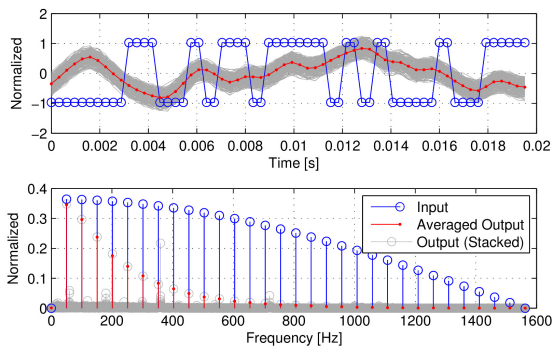

Figure 2: PRBS excitation signal of an orbit corrector and corresponding reading in a beam position monitor.

Each corrector was excited independently in order to simplify the identification process.

Input-Output Datasets

For orbit correctors, 42 datasets with 1 input (current setpoint) and 1 output (current reading) each were built from the acquired data. These datasets allowed black-box identification of discrete-time transfer functions in the form $Ga'_{pj}(z)=Ga_{pj}(z)H_d(z)$, that is, the combined response of power supply, magnet impedance, decimation filter and network delay.

For BPMs, 48 datasets with 1 input (filtered corrector current setpoint) and 1 output (beam position reading) each were built, where the orbit corrector to be excited was chosen as the corrector which produced the maximum static response at the BPM to be identified. The input data was then filtered by the identified model of the chosen orbit corrector resulting in the identification of the transfer function $H'_{pi}(z)=H_{pi}(z)Gp_{pj}(z)$, that is, the combined response of the i-th BPM and the magnet core plus vacuum chamber response of the j-th orbit corrector. Since the magnet core and vacuum chamber of all correctors were known to have bandwidth higher than 1.25 kHz, that is above the frequency range of interest (500 Hz), the $Gp_{pj}(z)$ dynamics were neglected.

Black-box Identification

Among several existing parametric black-box system identification methods, the Autoregressive model with Exogenous Inputs (ARX) was chosen [2]. In order to avoid biasing on the identification parameters, each dataset was averaged in time-domain: the output signals were segmented in 161 periods of 62 samples (approximately 3.2 s of data), being the first segment discarded to remove the transient dynamics. From the remaining segments, 80 segments were averaged and resulted in 62-sample long estimation dataset. Another 80 segments were averaged to form the validation dataset. Orbit corrector models of order 8 (16 coefficients) and delay of 3 sample times were used. BPM models of order 2 (4 coefficients) and delay of 1 sample time were used.

Figures 3a and 3b show the frequency response of the identified models for BPMs and orbit correctors, respectively.

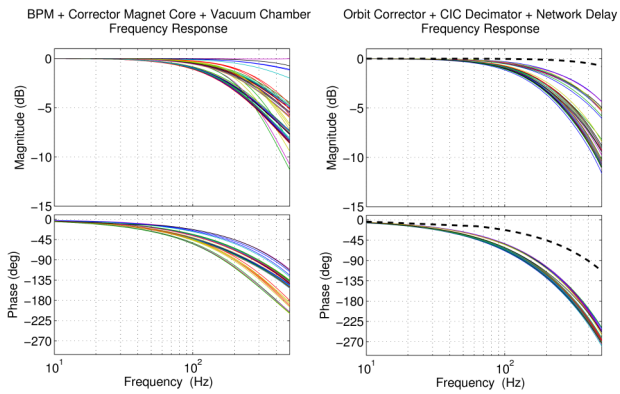

(a) (b)

Figure 3: Frequency responses of identified (a) BPM models, and (b) orbit corrector models. $H_d(z)$ frequency response is plotted in dashed black curve for comparison.

The identified models presented normalized root mean squared errors (NRMSE) above 91% and 97% for BPMs and orbit correctors, respectively (100% meaning perfect fit and 0 meaning the fit is as good as of a straight line equal to the mean of the data). Residual analysis showed no statistically significant correlation between estimation errors (residues) and the excitation signal for all the identified models.

CONTROL DESIGN

A signal-based H_2/H_∞ optimal control approach has been adopted when designing the FOFB controller. A fixed-structure controller requirement was imposed by the available hardware, making the synthesis of an optimal controller not possible by classical tools or not computationally efficient [3]. Robustness was analyzed using uncertain plant subsystem transfer functions and worst-case singular values frequency response plots.

ISBN 978-3-95450-148-9

Weights

The key element of a signal-based control design approach is to establish inputs, outputs and transfer function weights which directly express realistic disturbances, sensor noise, actuator noise and performance objectives [4]. Closed-loop optimization is then performed based on an augmented plant as illustrated in Fig. 4.

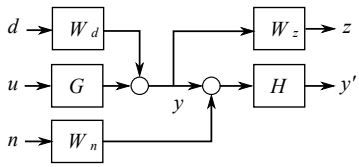

Figure 4: Augmented plant for signal-based control.

The blocks *G(z)* and *H(z)* are the plant and sensor matrix transfer functions, respectively, and $W_d(z)$, $W_n(z)$ and $W_z(z)$ are the weights for disturbance, noise and performance objectives.

In the case of the LNLS FOFB system, the $W_d(z)$ transfer function matrix was chosen to reflect the main electron beam disturbances on the UVX storage ring: (i) variation of EPU gap (ramp type); (ii) variation phase of EPU phase (ramp type); (iii) mains ripple from 60 Hz to 360 Hz (second order peak filters). By means of experiments, the orbit distortion profiles of each of these disturbances were obtained.

$W_n(z)$ was chosen as a diagonal transfer function matrix where each element is the worst-case (lowest beam current on operation conditions) standard deviation of the corresponding beam position measurement broadband noise integrated over the entire bandwidth.

$W_z(z)$ was chosen also as a diagonal matrix transfer function where each element is a first-order low pass filter with a given bandwidth and gain given by the inverse of the nominal beam size, meaning all beamlines are considered to be equally sensitive to electron beam orbit disturbances up to the bandwidth.

Actuator noise and amplitude range limitation were both considered to be negligible.

Performance and Robustness Metrics

FOFB performance and robustness were assessed by means of H_2 and H_∞ closed-loop system norms of the augmented plant, with negative feedback from $\boldsymbol{y'}$ to $\boldsymbol{u}$ by a controller with *C(z)* transfer function. The chosen performance channel was the summation of disturbance rejection and sensor noise transfer functions, with inputs $\boldsymbol{d}$ and $\boldsymbol{n}$ and output $\boldsymbol{z}$, denoted by $\|T_{d,n\to z}\|_2$, for which the H_2 norm has direct correspondence with the RMS-integrated criterion typically used to analyze FOFB system performance. The chosen robustness channel was the sensitivity transfer function at $\boldsymbol{y}$, denoted by $\|S_y\|_\infty$, for which the H_∞ norm simply means the worst-case multivariable gain from the disturbances to the actual beam position outputs. Despite being an indirect measure of robustness, it has straightforward practical meaning.

The H_2 and H_∞ norms were scaled in such a way that values below unity were said to satisfy the FOFB requirements. To this end, W_z was divided by a factor 0.1 to reflect 10% beam size stability requirement and by the square root of the number of beam position measurements (24, for each plane) in order to convert the 2-norm of the output vector to RMS value. Each input of W_d is divided by its expected maximum value, so that an unitary input means the worst-case disturbance. The sensitivity transfer function was divided by the allowed maximum amplification gain, $\sqrt{2}$ (3 dB).

Model Uncertainty

Despite adopting black-box system identification when modeling each BPM and orbit corrector dynamics, the transfer functions were assumed to have some level of uncertainty. In order to take this information into account when analyzing the control loop, classes of similar responses have been established from visual inspection followed by the determination of lower and upper bounds of the frequency responses through an input multiplicative uncertainty model of the type:

$$G_{uncertain}(z)=G_{nominal}(z)(1+W(z)\Delta(z)) \qquad (1)$$

where Δ(z) is a norm-bounded uncertain complex transfer function ($\|H(\Delta)\|_\infty<1$) and *W(z)* is a weighting transfer function of order 1. Figures 5a and 5b show the established frequency response classes.

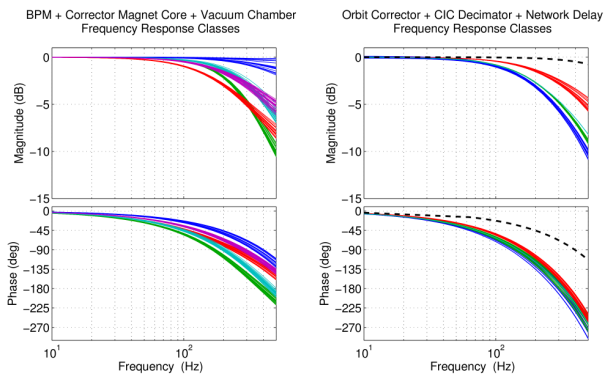

Figure 5: Classes of frequency responses of (a) BPM models, and (b) orbit corrector models. $H_d(z)$ frequency response is plotted in dashed black curve for comparison.

Control Optimization

Although mature frameworks for designing optimal controllers based on H_2 and H_∞ norms minimization exist (*e.g.* LQG, LMIs, μ-synthesis), these methods are not directly suitable for the LNLS FOFB system since the controller has a fixed-structure. For such class of controllers, optimizing the system norms would typically require nonconvex and nonsmooth optimization techniques. Although an efficient and scalable nonsmooth optimization method for solving this class of problems exists [3] and is available in Matlab Robust Control Toolbox since version 2010b, the present work has taken a simpler approach of exhaustive computation of system

ISBN 978-3-95450-148-9

norms for a grid of controller parameters. The next section describes simulation results which were obtained following this approach.

SIMULATION RESULTS

The feedback controller *C(z)* on the simulated control loops had the following structure:

$$C(z)=M_C\frac{K\cdot T_s}{z-1} \quad (2)$$

where M_C is a decoupling matrix, K is the controller gain and T_s is the sampling time (320 μs). M_C is the pseudo-inverse of the static orbit response matrix applying Tikhonov regularization as described in [5, 6]. The pseudo-inverse singular values $\hat{\sigma}_i$ have the following relation with the singular values of the orbit response matrix σ_i :

$$\hat{\sigma}_i=\frac{\sigma_i}{\sigma_i^2+\mu} \quad (3)$$

where μ is a real parameter to be tuned.

The closed-loop norms $\|T_{d,n\to z}\|_2$ and $\|S_y\|_\infty$ of the augmented plant (nominal case, with no uncertainty) were calculated for different values of K and μ for three different bandwidths in the $W_z(z)$ transfer function. Orbit correction on horizontal and vertical planes were treated independently. Figure 6 shows the results for each value of K, μ and bandwidth. The optimal controllers are those with minimum value of $\|T_{d,n\to z}\|_2$ meeting the constraint $\|S_y\|_\infty<1$, as summarized in Table 1.

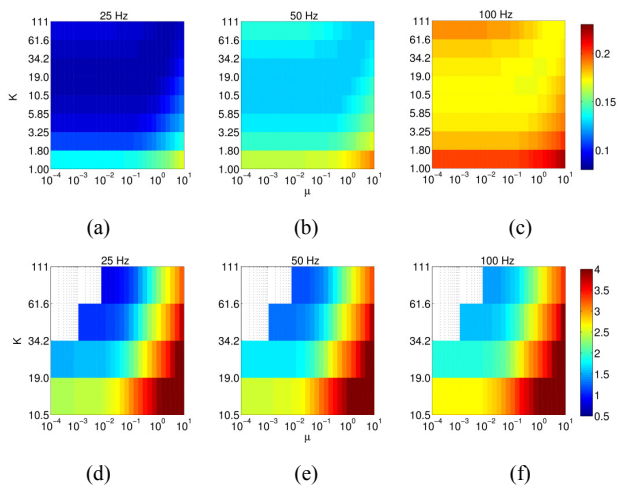

Figure 6: $\|T_{d,n\to z}\|_2$ costs meeting the $\|S_y\|_\infty<1$ constraint for each plane and beamline bandwidth: (a) horizontal, 25 Hz; (b) horizontal, 50 Hz; (c) horizontal, 100 Hz; (d) vertical, 25 Hz; (e) vertical, 50 Hz; (f) vertical, 100 Hz.

Table 1: Summary of optimal controllers.

Plane	BW	$\|T_{d,n\to z}\|_2$	$\|S_y\|_\infty$	K	μ
H	**25 Hz**	0.0855	0.7467	19.0	4.17e-1
H	**50 Hz**	0.1271	0.7294	10.5	2.81e-1
H	**100 Hz**	0.1710	0.7293	10.5	4.17e-1
V	**25 Hz**	0.7837	0.9746	111	1.17e-2
V	**50 Hz**	1.160	0.8585	61.6	5.30e-3
V	**100 Hz**	1.466	0.8480	61.6	7.88e-3

Figure 7 shows the frequency-dependent singular values of the sensitivity transfer function of the system for each controller in Table 1. The uncertainty on dynamics and orbit response matrix is taken into account. No closed-loop sensitivity function of the optimized loops significantly exceeds the 3 dB amplification reference line, indicating the uncertainties do not substantially degrade robustness. This was expected since the differences on dynamics are significant only for frequencies above the achieved closed-loop bandwidths.

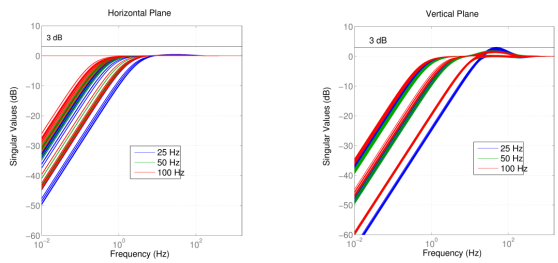

Figure 7: Singular values plot of sensitivity functions with uncertain plant: (a) Horizontal plane (b)Vertical plane.

CONCLUSION

A complete approach to identify the performance limits of the LNLS FOFB system has been presented, from the system identification to the control loop optimization. From this study it has been concluded that the LNLS FOFB system is limited in about 15 Hz closed-loop bandwidth (~25 Hz 0 dB crossover on sensitivity function), the main limitation being a ~1.5 ms delay due to communication network, decimation filters and BPMs responses. Due to the effect of noise amplification for frequencies above the crossover, higher control loop bandwidths improves performance only when beamlines are less sensitive to electron beam motion at higher bandwidths. The simulation results herein presented still need to be validated against experimental data.

REFERENCES

[1] L. Sanfelici et al., "LNLS Fast Orbit Feedback System", MOP263, PAC'11.

[2] L. Ljung, *System Identification: Theory for the User, 2nd edition*, (New Jersey: Prentice-Hall, 1999).

[3] P. Apkarian et al., "Nonsmooth optimization algorithm for mixed H_2/H_∞ synthesis", Conference on Decision and Control 2007.

[4] S. Skogestad and I. Postlethwaite, *Multivariable Feedback Control: Analysis and Design, 2nd edition*, (Chichester: Wiley, 2005).

[5] J. Rowland et al., "Status of the Diamond Fast Orbit Feedback System", RPPA10, ICALEPCS'07.

[6] S. Gayadeen et al., "Fast Orbit Feedback Control in Mode Space", THMIB07, ICALEPCS'13.

ISBN 978-3-95450-148-9